Eur. J. Mineral., 37, 319–335, 2025
https://doi.org/10.5194/ejm-37-319-2025

European Journal of Mineralogy
Open Access

Ginelfite, $Ag_2(Ag_{0.5}Fe_{0.5})TlPb_{24.5}(Sb,As)_{32.5}S_{75.5}$, a new boxwork sulfosalt from Jas Roux, France: occurrence and crystal structure

Cristian Biagioni[1,2], Jiří Sejkora[3], Yves Moëlo[4], Georges Favreau[a], Vincent Bourgoin[b], Jean-Claude Boulliard[5], Elena Bonaccorsi[1,2], Daniela Mauro[1,6], Silvia Musetti[1], Marco Pasero[1,2], Natale Perchiazzi[1,2], and Jana Ulmanová[3]

[1]Dipartimento di Scienze della Terra, Università di Pisa, Via Santa Maria, 53, 56126 Pisa, Italy
[2]Centro per l'Integrazione della Strumentazione Scientifica dell'Università di Pisa (CISUP), Università di Pisa, 56126 Pisa, Italy
[3]Department of Mineralogy and Petrology, National Museum, Cirkusová 1740, 193 00, Prague 9, Czech Republic
[4]Nantes University, CNRS, Institut des Matériaux Jean Rouxel, IMN, 44000 Nantes, France
[5]Collection des Minéraux de Jussieu, IMPMC, Université Pierre et Marie Curie, Case courrier 73, 4 Place Jussieu, 75252 Paris CEDEX 05, France
[6]Museo di Storia Naturale, Università di Pisa, Via Roma 79, 56011 Calci, Italy
[a]current address: 421 Avenue Jean Monnet, 13090 Aix-en-Provence, France
[b]current address: 32 Avenue Ernest Renan, 95210 Saint-Gratien, France

Correspondence: Cristian Biagioni (cristian.biagioni@unipi.it)

Received: 23 September 2024 – Revised: 1 March 2025 – Accepted: 3 March 2025 – Published: 21 May 2025

Abstract. Ginelfite, $Ag_2(Ag_{0.5}Fe_{0.5})TlPb_{24.5}(Sb,As)_{32.5}S_{75.5}$ ($Z = 2$), was discovered in the hydrothermal deposit of Jas Roux, Hautes-Alpes, France, as dark grey, metallic, acicular crystals up to 0.5 mm long, associated with sphalerite and lopatkaite in a baryte + quartz gangue. In reflected light, ginelfite is light grey, with weak pleochroism and bireflectance. Anisotropism is moderate, with weak brownish and blue tints. Reflectance data for the four COM wavelengths in air (λ (nm): R_{min}/R_{max} (%)) are 470: 35.4/38.1; 546: 34.6/37.0; 589: 33.7/36.0; 650: 32.3/34.6. Electron microprobe analysis gave (in wt% – average of 35 spot analyses) Cu 0.07, Ag 2.34, Tl 1.14, Pb 45.44, Fe 0.22, As 6.17, Sb 23.46, S 21.07, total 99.91. On the basis of $\Sigma Me = 61$ apfu (atoms per formula unit), the empirical formula of ginelfite is $Cu_{0.12}Ag_{2.51}Fe_{0.46}Tl_{0.65}Pb_{25.40}Sb_{22.32}As_{9.54}S_{76.12}$. Ginelfite is triclinic, space group $P\bar{1}$, with unit-cell parameters $a = 8.3635(6)$ Å, $b = 27.5481(19)$ Å, $c = 29.199(2)$ Å, $\alpha = 95.335(3)°$, $\beta = 94.123(3)°$, $\gamma = 94.367(3)°$, and $V = 6657.7(8)$ Å^3. The crystal structure was solved and refined by single-crystal X-ray diffraction data to a final $R_1 = 0.0876$ on the basis of 23 779 unique reflections with $F_o > 4\sigma(F_o)$ and 1158 refined parameters. Ginelfite is a new rod-based Ag–Tl–Pb sulfosalt showing a boxwork organization. The name ginelfite honours Carlo Gini (born 1954) and Francesco Guelfi (born 1947), former technicians at the X-ray laboratory of the University of Pisa for their contributions to the development of the mineralogical research in Pisa during the last 40 years.

1 Introduction

The hydrothermal deposit of Jas Roux (France) is one of the most interesting European localities for the study of the mineralogy of the element Tl ($Z = 81$), along with other localities such as Lengenbach (Switzerland – Raber and Roth, 2018), Allchar (North Macedonia – Boev et al., 2001-2002), and Monte Arsiccio (Italy – Biagioni et al., 2020). At Jas Roux, the Tl–Hg–Ag–Sb–As mineralization occurs within baryte layers, mainly hosted in metadolostone and marble. Johan and Mantienne (2000) gave a full account of the mineralogy of this ore deposit, updated by Bourgoin et al. (2011) who cited 57 different mineral species. The Jas Roux deposit is currently known for the occurrence of 11 Tl-bearing species. Among them, seven have their type locality there, i.e. chabournéite (Johan et al., 1981), dewitite (Topa et al., 2020), écrinsite (Topa et al., 2017), markwelchite (Bindi et al., 2024), pierrotite (Guillemin et al., 1970), routhierite (Johan et al., 1974), and vallouiseite (Topa et al., 2023b). Moreover, Jas Roux is the type locality of the Ag sulfosalts jasrouxite (Topa et al., 2013a), laffittite (Johan et al., 1974), and montpelvouxite (Topa et al., 2023e). In addition to these species, some unnamed minerals were described by Johan and Mantienne (2000). Two of them are reported in the list of Valid Unnamed Minerals (Smith and Nickel, 2007) as UM2000-44-S:AgAsPbSb and UM2000-45-S:AgAsSb.

During the investigation of a suite of specimens collected by three of us (Georges Favreau, Jean-Claude Boulliard, and Vincent Bourgoin) during a sampling campaign authorized by the Écrins National Park, some acicular crystals characterized by the occurrence of Ag, Tl, Pb, Sb, As, S, and minor Fe were identified. An X-ray powder diffraction pattern revealed a close match between this unknown phase and the unnamed mineral UM2000-44-S:AgAsPbSb (Smith and Nickel, 2007), first reported by Mantienne (1974) and later examined by Moëlo (1983) and Johan and Mantienne (2000). Notwithstanding the relatively low quality of the single-crystal X-ray diffraction patterns collected using the new available material, the crystal structure was solved and refined, fitting with the quantitative chemical data obtained through electron microprobe analysis. In this way, a consistent set of data allowed for the proposal of the new mineral species ginelfite. This name honours Carlo Gini (born 1954) and Francesco Guelfi (born 1947), former technicians at the X-ray laboratory of the Dipartimento di Scienze della Terra of the Università di Pisa (Carlo Gini from 1988 to 2019, Francesco Guelfi from 1981 to 2011) for their invaluable contribution to the development of the mineralogical research carried out in Pisa over the last 40 years. Besides, the naming also intends to acknowledge the fundamental role played by lab technicians all around the world in supporting researchers in mineralogy. The name ginelfite is formed by a combination of their surnames.

The new mineral and its name have been approved by the Commission on New Minerals, Nomenclature and Classification of the International Mineralogical Association, under the voting number 2022-110. Its mineral symbol, in accord with Warr (2021), is Glf. Holotype material of ginelfite is deposited in the collections of the Museo di Storia Naturale of the Università di Pisa, Via Roma 79, 56011 Calci (PI), under catalogue number 20023, and in the collections of the Department of Mineralogy and Petrology, National Museum in Prague, Cirkusová 1740, 193 00 Prague 9, Czech Republic, under catalogue number P1P 31/2022.

In this paper, the occurrence, physical properties, and crystal structure of ginelfite are described.

2 Occurrence and physical properties

Ginelfite was found at the Tl-rich hydrothermal deposit of Jas Roux, La Chapelle-en-Valgaudémar, Hautes-Alpes department, France (geographic coordinates: 44°44′45″ N, 6°19′18″ E). Type material was sampled from the centre of the cliff of the tectonic block indicated as "compartiment 2" by Mantienne (1974). In this block, the Tl-bearing mineralization occurs within a 3.8 m thick baryte-rich zone (Johan and Mantienne, 2000). This area is also the type locality for the recently described new species dewitite, écrinsite, jasrouxite, markwelchite, montpelvouxite, and vallouiseite (Bindi et al., 2024; Topa et al., 2013a, 2017, 2020, 2023b, e).

Ginelfite occurs as acicular crystals, up to 0.5 mm in length, dark grey in colour, with black streaks and metallic lustre (Fig. 1). Mohs hardness was not measured, owing to the small size of the studied grains. Johan and Mantienne (2000) reported a $VHN_{25} = 165\,kg\,mm^{-2}$ for five indentations (range 157–170 $kg\,mm^{-2}$) measured on five different grains. These values correspond to a Mohs hardness of 3–$3\frac{1}{2}$. Ginelfite is brittle, with a conchoidal fracture. Cleavage was not observed. Owing to the small amount of available material, density was not measured. Based on the empirical formula and unit-cell parameters derived from single-crystal X-ray diffraction, the calculated density is 5.765 $g\,cm^{-3}$.

Ginelfite is opaque. In reflected light, it is light grey. Pleochroism and bireflectance are weak. It is moderately anisotropic, with weak brownish and blue tints. Internal reflections were not observed. Reflectance values (Table 1) were measured in air using a MSP400 TIDAS spectrophotometer at a Leica microscope, with a 50× objective and WTiC Zeiss 370 standard. The reflectance curves for ginelfite are shown in Fig. 2, along with data for UM2000-44-S:AgAsPbSb (Johan and Mantienne, 2000), whose data are also given in Table 1. Lower values of R_{max} of ginelfite may be caused by a limited number of ginelfite sections in the studied sample.

In type material, ginelfite is associated with sphalerite (occurring as pale brownish grains, Fe-poor, and with trace amounts of Cd) and with lopatkaite within a silicified matrix, devoid of vugs, with baryte and quartz.

Table 1. Reflectance data for ginelfite, compared with data for UM2000-44-S:AgAsPbSb (after Johan and Mantienne, 2000).

Ginelfite		UM2000-44-S:AgAsPbSb			Ginelfite		UM2000-44-S:AgAsPbSb		
R_{max}	R_{min}	R_{max}	R_{min}	λ (nm)	R_{max}	R_{min}	R_{max}	R_{min}	λ (nm)
38.9	35.7	–	–	400	36.7	34.3	39.7	34.5	560
38.9	36.1	43.7	38.6	420	36.3	33.9	39.3	33.9	580
38.6	35.9	43.2	38.0	440	**36.0**	**33.7**	–	–	**589**
38.2	35.5	42.5	37.1	460	35.8	33.5	38.4	33.3	600
38.1	**35.4**	–	–	**470**	35.4	33.0	37.8	32.7	620
37.9	35.3	41.9	36.6	480	34.9	32.6	37.0	32.1	640
37.6	35.1	41.4	36.0	500	**34.6**	**32.3**	–	–	**650**
37.3	34.9	41.1	35.5	520	34.4	32.1	36.2	31.4	660
37.0	34.6	40.4	35.0	540	34.0	31.7	35.2	30.5	680
37.0	**34.6**	–	–	**546**	33.4	31.2	34.5	30.0	700

Note: the four COM values are shown in bold.

3 Experimental

3.1 Chemical analysis

Quantitative chemical analyses of ginelfite were carried out using a Cameca SX 100 electron microprobe (National Museum of Prague, Czech Republic) and the following experimental conditions: WDS mode, accelerating voltage of 25 kV, beam current of 20 nA, and beam diameter of 1 µm. Standards (element, emission line) were Ag (Ag$L\alpha$), chalcopyrite (Cu$K\alpha$, S$K\alpha$), NiAs (As$L\beta$), PbS (Pb$M\alpha$), pyrite (Fe$K\alpha$), Sb_2S_3 (Sb$L\alpha$), and Tl(Br,I) (Tl$L\alpha$). Contents of other sought elements with atomic numbers greater than 8 are below detection limits. Matrix correction by the PAP algorithm (Pouchou and Pichoir, 1985) was applied to the data. Results are given in Table 2.

Five spot analyses were performed on associated lopatkaite (Fig. 1b). The average of these latter analyses is (in wt%) Pb 55.82(29), As 3.80(8), Sb 20.98(8), S 19.93(6), total 100.52(30).

3.2 X-ray crystallography

X-ray powder diffraction data of ginelfite (Table 3) were collected using a 114.6 mm Gandolfi camera with Ni-filtered Cu$K\alpha$ radiation.

Several acicular crystals were extracted from the available specimen and were checked to find a sample suitable for the single-crystal X-ray diffraction study. Single-crystal X-ray diffraction intensity data of ginelfite were collected using a Bruker D8 Venture four-circle diffractometer, equipped with an air-cooled Photon III detector and microfocus Mo$K\alpha$ radiation (Centro per l'Integrazione della Strumentazione Scientifica dell'Università di Pisa, CISUP, Università di Pisa, Pisa, Italy). The detector-to-crystal distance was set to 41 mm. Data were collected using φ and ω scan modes, in 0.5° slices, with an exposure time of 60 s per frame. A total of 3091 frames was collected, and frames were integrated with the Bruker SAINT software package using a narrow-frame algorithm. Data were corrected for Lorentz-polarization, absorption, and background. Unit-cell parameters were refined on the basis of the XYZ centroids of 9656 reflections above $20\sigma(I)$ with $5.04° < 2\theta < 54.92°$ as $a = 8.3635(6)$ Å, $b = 27.5481(19)$ Å, $c = 29.199(2)$ Å, $\alpha = 95.335(3)°$, $\beta = 94.123(3)°$, $\gamma = 94.367(3)°$, $V = 6657.7(8)$ Å^3, space group $P-1$.

The crystal structure of ginelfite was solved using ShelxT (Sheldrick, 2015a) and refined through Shelxl-2018 (Sheldrick, 2015b). Site occupancy factors were modelled using neutral scattering curves taken from the *International Tables for Crystallography* (Wilson, 1992). One-hundred and thirty-seven independent atom positions were found in the crystal structure of ginelfite, corresponding to 61 cation and 76 anion sites. Among cation positions, 21 are pure Pb sites, 1 is a mixed (Tl,Pb) position, 12 are mixed (Pb / Sb) sites, and 24 have an (Sb / As) occupancy, with variable Sb / (Sb + As) atomic ratios. The three remaining cation sites host Ag atoms (two sites) or show a mixed (Ag / Fe) occupancy. All 76 anion positions are occupied by S atoms. The site occupancies of mixed sites were initially refined, with the only fixed-site occupancy being that of the (Tl,Pb) position, based on bond-valence sums and agreeing with chemical data. An examination of the bond-valence sum (BVS) for all atoms, using ECoN21 (Ilinca, 2022), showed several underbonded or overbonded cations. Whereas in some cases underbonding could be due to the average nature of the refined positions, overbonding was more serious and some (Sb / As) sites had a BVS of up to ca. 4.0 valence units (v.u.). Consequently, the occupancy of some mixed positions was adjusted to optimize their BVS. In the case of split and mixed positions, after an initial refinement of the mean atomic number (MAN, as defined in Hawthorne et al., 1995), the site occupancies were adjusted by considering not

Table 2. Chemical data (in wt%) for ginelfite and UM2000-44-S:AgAsPbSb.

Element	wt%	Range ($n = 35$)	e.s.d.	[1]	[1]	[2]	[2]	[2]
Cu	0.07	0.00–0.09	0.02	–	–	b.d.l.	b.d.l.	b.d.l.
Ag	2.34	2.20–2.42	0.05	2.4	2.6	2.54	2.58	2.45
Tl	1.14	0.98–1.34	0.09	n.a.	3.1	2.57[a]	2.51	2.63
Pb	45.44	44.81–45.83	0.21	44.0	43.6	43.14	42.03	42.12
Fe	0.22	0.20–0.25	0.01	n.a.	n.a.	0.19	0.19[b]	0.19[b]
As	6.17	5.84–6.48	0.17	5.2	8.5	4.86	5.35	5.36
Sb	23.46	23.10–23.94	0.19	26.0	22.4	25.15	25.38	24.83
S	21.07	20.62–21.32	0.14	20.8	20.8	21.04	20.72	20.30
Total	99.91	99.21–100.59	0.32	98.4	101.0	99.49	98.76	97.88
apfu ($\Sigma Me = 61$)								
Cu	0.12	0.00–0.17	0.04	–	–	–	–	–
Ag	2.51	2.38–2.61	0.05	2.62	2.69	2.77	2.79	2.68
Tl	0.65	0.56–0.76	0.05	n.a.	1.69	1.48	1.43	1.52
Pb	25.40	25.14–25.70	0.14	25.03	23.46	24.46	23.69	23.95
Fe	0.46	0.41–0.52	0.03	n.a.	n.a.	0.40	0.40	0.40
As	9.54	9.05–9.97	0.24	8.18	12.65	7.62	8.34	8.43
Sb	22.32	21.91–22.67	0.18	25.17	20.51	24.27	24.34	24.03
S	76.12	74.14–77.04	0.74	76.45	72.32	77.10	75.47	74.59
Ev(%)	−1.1	−2.3–+1.7	1.0	−0.1	+4.2	−2.9	−0.3	+0.7
Sb + As	31.86	31.60–32.08	0.12	33.35	33.16	31.89	32.68	32.46
Sb / (Sb + As)	0.701	0.689–0.715	0.007	0.755	0.619	0.761	0.745	0.740
Pb_{corr}	26.70	26.40–27.01	0.14	25.03	26.84	27.42	26.56	26.98
Sb_{corr}	31.21	30.89–31.49	0.12	33.35	31.47	30.41	31.25	30.94
Pb_{corr} / Sb_{corr}	0.855	0.838–0.875	0.007	0.751	0.853	0.902	0.850	0.872

Note: n represents the number of spot analyses; e.s.d. represents estimated standard deviation; $Pb_{corr} = Pb + 2Tl$; $Sb_{corr} = Sb + As - Tl$. [1] Mantienne (1974); [2] Moëlo (1983). [a]not analysed and assumed as an average of the other two analyses; [b]Fe content according to the first analysis.

only the refined MAN, but also the observed bond lengths and BVS. Some mixed cation positions and some S atoms were modelled isotropically, to avoid negatively defined displacement parameters. Moreover, the examination of bond-valence sums and displacement parameters suggested that one S site, namely the S(71) site, could be partially occupied. Finally, the occurrence of twinning according to a [100] twofold axis (twin obliquity 5.8°) was modelled. The ratio between the two twin components refined to 62.2 : 37.8(2). It is worth noting that attempts to refine the crystal structure on the major component, after the change in atomic coordinates, or the use of the HKLF5 method (e.g. Bolte, 2004) did not improve the refinement (which was slightly worse in both cases). The structural model converged to $R_1 = 0.0876$ for 23 779 reflections with $F_o > 4\sigma(F_o)$ and 1158 refined parameters. Details of data collection and refinement are given in Table 4. Site occupancy factors, fractional atomic coordinates, and displacement parameters, as well as bond distances, can be found in the Crystallographic Information File (CIF), deposited in the Supplement, whereas site occupancies, average bond distances, and bond-valence sums at cation sites are given in Table 5. Bond-valence sums at anion positions are shown in Table 6.

4 Results and discussions

4.1 Chemical formula

The recalculation of the chemical formula of ginelfite is not straightforward. Indeed, on the basis of the results of the structural analysis (see below), it seems reasonable to normalize the chemical formula on the basis of $\Sigma Me = 61$ atoms per formula unit (apfu). However, it is not clear if Cu should be considered among these atoms or if it could occur in a low-occupied position, as observed, for instance, in nuffieldite and zinkenite (Moëlo et al., 1997; Biagioni et al., 2018a). As no maxima interpretable as tetrahedrally coordinated Cu could be found in the difference Fourier maps, it was assumed that Cu replaces Ag at the tetrahedrally coordinated sites (see below); consequently, it was counted among the 61 apfu. The empirical formula of ginelfite is $Cu_{0.12(4)}Ag_{2.51(5)}Fe_{0.46(3)}Tl_{0.65(5)}Pb_{25.40(14)}Sb_{22.32(18)}As_{9.54(24)}S_{76.12(74)}$. The relative error on valence equilibrium Ev(%), defined as $[Ev(+) - Ev(-)] \times 100 / Ev(-)$, is

Table 3. Observed and calculated X-ray powder diffraction data for ginelfite. Intensity and d_{hkl} were calculated using the software PowderCell 2.3 (Kraus and Nolze, 1996) on the basis of the structural model given in the Crystallographic Information File. Only reflections with $I_{calc} > 10$ are listed (if not observed). The seven strongest reflections are given in bold.

d_{obs}	I_{obs}	I_{calc}	d_{calc}	$h\ k\ l$	d_{obs}	I_{obs}	I_{calc}	d_{calc}	$h\ k\ l$	d_{obs}	I_{obs}	I_{calc}	d_{calc}	$h\ k\ l$
		10	8.455	0 3 1			14	3.355	0 8 1			10	2.735	−2 8 1
		11	7.544	0 2 3			58	3.340	0 −4 8			11	2.734	2 7 0
		15	6.982	0 −3 3			37	3.227	0 −6 7	**2.729**	**ms**	19	2.733	0 10 0
		18	4.432	0 6 1	3.197	w	12	3.220	0 0 9			17	2.732	−2 7 4
		15	4.225	0 6 2	3.110	w	10	3.136	2 −6 2			10	2.732	2 −4 7
4.168	w	15	4.161	2 −1 0			15	3.136	−2 −5 3			20	2.731	2 6 3
		13	4.161	2 −1 0			11	3.085	2 2 5			11	2.662	0 5 9
		57	4.103	0 3 6	3.056	w	35	3.077	0 4 8	2.658	w	12	2.650	−2 0 9
3.875	w	23	3.905	0 7 0			32	3.052	0 −9 1			10	2.649	2 −1 8
		17	3.868	0 −7 2			32	2.983	0 −6 8	2.611	vw	5	2.614	2 −3 8
		10	3.812	0 −5 6			12	2.962	2 −7 1			7	2.450	−2 9 3
		12	3.767	0 −6 5			13	2.962	−2 −6 2	2.452	w	7	2.449	2 8 2
3.698	w	35	3.707	0 −4 7			13	2.960	−2 −4 6			6	2.447	−2 −2 10
		12	3.663	−2 3 3	**2.965**	**s**	15	2.960	2 −5 5			7	2.446	2 −3 9
		13	3.636	0 3 7			32	2.957	−2 4 6	2.373	w	7	2.377	2 −10 1
		13	3.626	−2 2 4			34	2.956	2 3 5			6	2.376	−2 −9 2
3.604	w	19	3.623	0 0 8			14	2.941	2 −6 4	2.291	w	12	2.294	−2 1 11
		11	3.582	−2 −2 4			16	2.922	−2 −6 3			11	2.293	2 0 10
		19	3.562	2 −4 2			12	2.903	0 −5 9	2.214	vw	8	2.230	0 −11 7
		18	3.561	−2 −3 3			11	2.901	−2 7 2			9	2.206	0 11 5
		13	3.502	0 7 3			12	2.888	−2 3 7	2.169	w	11	2.168	2 −10 6
		13	3.487	0 −3 8			12	2.887	2 2 6	**2.091**	**vs**	100	2.091	−4 1 1
		11	3.450	2 −5 0			14	2.845	−2 0 8	2.038	vw	5	2.034	2 −2 12
		12	3.449	−2 −4 1			15	2.844	2 −1 7	2.001	vw	9	2.021	0 −12 8
		19	3.433	0 −8 1			43	2.826	−2 7 3	1.983	vw	9	1.979	2 10 5
		23	3.428	−2 −3 4			41	2.825	2 6 2	1.939	vw	8	1.932	0 0 15
		26	3.428	2 −4 3	**2.805**	**ms**	13	2.816	−2 −5 6	**1.872**	**ms**	17	1.873	2 −13 5
3.413	**s**	48	3.417	0 8 0			17	2.816	2 −6 5			15	1.873	−2 −12 6
		84	3.395	0 4 7			20	2.779	−2 4 7	1.820	w	5	1.821	4 −5 6
		28	3.393	−2 −2 5			21	2.778	2 3 6	**1.785**	**ms**	13	1.780	4 3 6
		27	3.393	2 −3 4										

Note: vs = very strong; s = strong; ms = medium-strong; w = weak; vw = very weak.

−1.1(1.0), assuming Fe as Fe^{2+}; this value is −0.8(1.0) if Fe occurs as Fe^{3+}. The actual oxidation state of Fe is difficult to assess, and no direct measurements were possible, owing to the low amount of available material and the low concentration of Fe in ginelfite (i.e. 0.22 wt%).

4.1.1 Chemical formula of associated lopatkaite

Lopatkaite is a homeotype of boulangerite reported by Topa et al. (2013b) from Madoc, Canada. Its type description has not been published yet. For the sake of completeness, the chemical formula of lopatkaite associated with ginelfite, calculated on the basis of 20 apfu, is $Pb_{4.84(3)}Sb_{3.09(1)}As_{0.91(2)}S_{11.16(3)}$, $Ev(\%) = -2.8(6)$.

4.2 Crystal structure description

4.2.1 Atom coordination

As briefly reported above, in the crystal structure of ginelfite there are 21 pure Pb sites, 1 mixed (Tl,Pb) position, 12 mixed (Pb / Sb) sites, 24 (Sb / As) sites with variable Sb /(Sb+As) ratios, 2 pure Ag positions, and 1 mixed (Ag / Fe) site. Figure 3 shows the unit-cell content of ginelfite.

Lead and thallium sites

Lead atoms show different coordination environments. Twelve Pb atoms, hosted at the Pb(1)–Pb(12) sites, display a "standing" bicapped trigonal prismatic coordination, with average <Pb–S> distances ranging from 3.08 to 3.12 Å, with BVS varying between 1.78 and 1.95 v.u. Pb(1)–Pb(6) and Pb(7)–Pb(12) sites form two symmetry-independent triangular columns. Lead atoms hosted at the Pb(13), Pb(15),

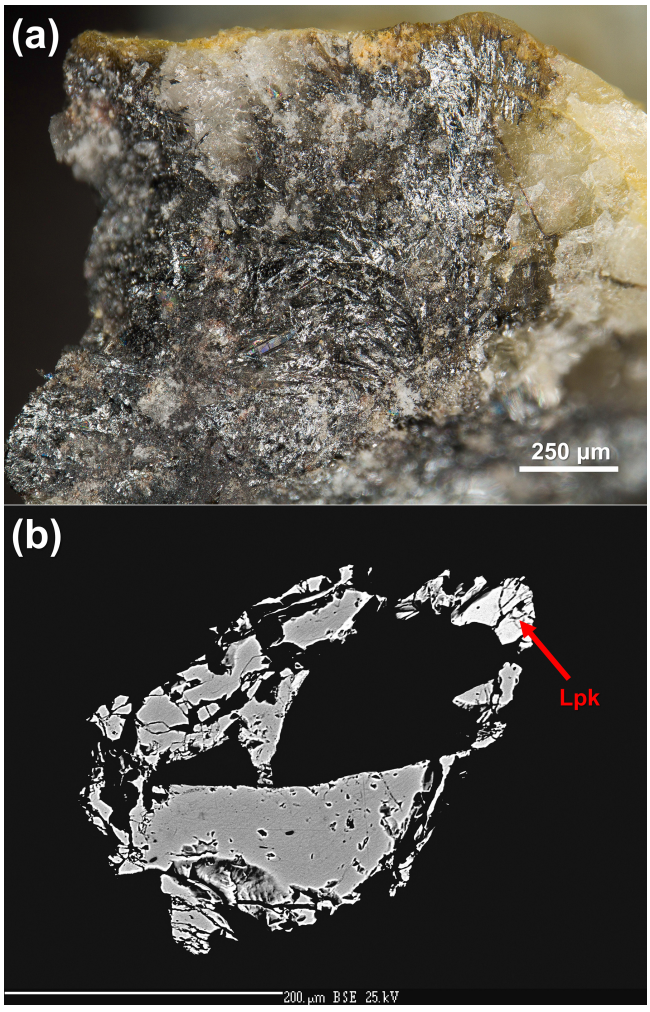

Figure 1. **(a)** Ginelfite, as dark grey acicular crystals with quartz and baryte. Photo Vincent Bourgoin. **(b)** Backscattered electron (BSE) image of the grain used for electron microprobe and reflectance measurements. White domains correspond to lopatkaite (Lpk).

Pb(16), and Pb(17) sites have a "lying-down" monocapped trigonal prismatic coordination, with average <Pb–S> distance of ca. 3.00 Å and BVS from 2.08 to 2.16 v.u., whereas Pb(14) and Pb(18) have a lying-down distorted octahedral coordination, with average <Pb–S> of ca. 3.01 Å and BVS of 1.87 and 1.97 v.u., respectively. Finally, a ninefold coordination, corresponding to a standing tricapped trigonal prism around the Pb atom, is shown by Pb(19), Pb(21), and Pb(22), with average <Pb–S> distances in the range 3.17–3.20 Å and BVS between 1.67 and 1.93 v.u. The ninefold-coordinated Tl(20) site corresponds to a tricapped trigonal prism and shows a <Tl–S> distance of 3.29 Å, definitely longer than those shown by Pb-hosting sites. Its BVS is 1.30 v.u., and it agrees with the site occupancy $(Tl_{0.65}Pb_{0.35})$ suggested by electron microprobe data.

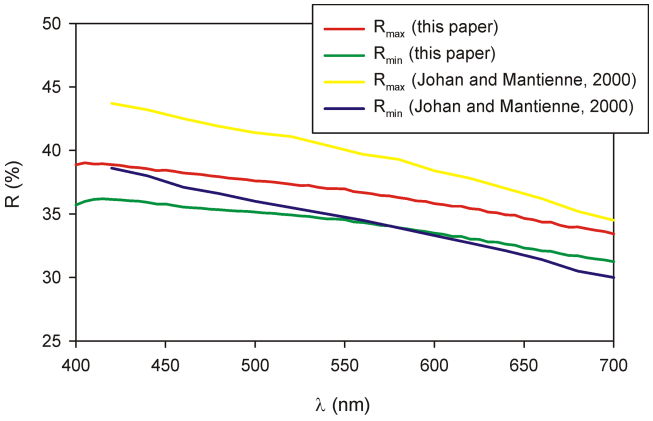

Figure 2. Reflectance curve for ginelfite compared with data for UM2000-44-S:AgAsPbSb (after Johan and Mantienne, 2000).

Table 4. Crystal and experimental data for ginelfite.

Crystal data	
Crystal size (mm)	0.060 × 0.015 × 0.015
Cell setting, space group	Triclinic, $P-1$
a (Å)	8.3635(6)
b (Å)	27.5481(19)
c (Å)	29.199(2)
α (°)	95.335(3)
β (°)	94.123(3)
γ (°)	94.367(3)
V(Å^3)	6657.7(8)
Z	2
Data collection and refinement	
Radiation, wavelength (Å)	Mo$K\alpha$, $\lambda = 0.71073$
Temperature (K)	293(2)
$2\theta_{max}$ (°)	54.99
Measured reflections	291 055
Unique reflections	30 492
Reflections with $F_o > 4\sigma(F_o)$	23 779
R_{int}	0.0515
$R\sigma$	0.0261
Range of h, k, l	$-10 \le h \le 10$, $-35 \le k \le 35$, $-37 \le l \le 37$
$R[F_o > 4\sigma(F_o)]$	0.0876
R (all data)	0.1131
wR (on F_o^2)	0.1764
Goof	1.221
Number of least-square parameters	1158
Maximum and minimum residual peak (e Å^{-3})	9.23 (at 0.22 Å from Pb(20)) −8.16 (at 0.14 Å from $M(7)$)

Mixed lead–antimony sites

Mixed (Pb / Sb) sites can be divided into Pb-dominant and Sb-dominant positions. Three sites have $Pb_{occ.} > Sb_{occ.}$ (where subscript occ. indicates the Pb and Sb occupancy), i.e. $M(1)$, $M(5)$, and $M(6)$. Lead atoms at $M(1)$ show a distorted octahedral coordination, with a seventh very long

Table 5. Site occupancy (s.o.), average bond distances (in Å), and bond-valence sums (in v.u.) for cations in ginelfite.

Site	s.o.	<*Me*–S>	BVS	Site	s.o.	<*Me*–S>	BVS
Pb(1)	$Pb_{1.00}$	3.107	1.90	*M*(10b)	$Sb_{0.37}Pb_{0.16}$	3.068	1.51
Pb(2)	$Pb_{1.00}$	3.125	1.78	*M*(11a)	$Pb_{0.41}Sb_{0.27}$	3.151	1.73
Pb(3)	$Pb_{1.00}$	3.086	1.90	*M*(11b)	$Sb_{0.19}Pb_{0.13}$	3.004	0.86
Pb(4)	$Pb_{1.00}$	3.109	1.89	*M*(12a)	$Sb_{0.07}$	2.944	0.21
Pb(5)	$Pb_{1.00}$	3.115	1.84	*M*(12b)	$Sb_{0.80}Pb_{0.13}$	2.956	2.74
Pb(6)	$Pb_{1.00}$	3.081	1.93	Sb(1)	$Sb_{1.00}$	2.571	2.76
Pb(7)	$Pb_{1.00}$	3.088	1.90	As(2)	$As_{0.50}Sb_{0.50}$	2.414	3.02
Pb(8)	$Pb_{1.00}$	3.080	1.95	As(3)	$As_{0.75}Sb_{0.25}$	2.351	2.99
Pb(9)	$Pb_{1.00}$	3.088	1.93	As(4)	$As_{0.90}Sb_{0.10}$	2.302	3.06
Pb(10)	$Pb_{1.00}$	3.094	1.88	Sb(5)	$Sb_{1.00}$	2.582	3.00
Pb(11)	$Pb_{1.00}$	3.079	1.94	Sb(6)	$Sb_{0.53(3)}As_{0.47(3)}$	2.419	2.97
Pb(12)	$Pb_{1.00}$	3.087	1.95	Sb(7)	$Sb_{1.00}$	2.824*	2.78
Pb(13)	$Pb_{1.00}$	3.005	2.13	As(8)	$As_{0.80}Sb_{0.20}$	2.391	3.06
Pb(14)	$Pb_{1.00}$	3.010	1.87	Sb(9)	$Sb_{0.90}As_{0.10}$	2.497	3.04
Pb(15)	$Pb_{1.00}$	3.009	2.08	Sb(10)	$Sb_{1.00}$	2.569	2.80
Pb(16)	$Pb_{1.00}$	3.007	2.07	Sb(11)	$Sb_{0.64(3)}As_{0.36(3)}$	2.470	3.23
Pb(17)	$Pb_{1.00}$	3.000	2.16	As(12)	$As_{0.60}Sb_{0.40}$	2.832*	2.98
Pb(18)	$Pb_{1.00}$	3.007	1.97	As(13)	$As_{0.60}Sb_{0.40}$	2.415	2.99
Pb(19)	$Pb_{1.00}$	3.193	1.93	Sb(14)	$Sb_{1.00}$	2.955*	2.74
Tl(20)	$Tl_{0.65}Pb_{0.35}$	3.291	1.30	As(15)	$As_{0.85}Sb_{0.15}$	2.538*	3.20
Pb(21)	$Pb_{1.00}$	3.202	1.82	Sb(16)	$Sb_{1.00}$	2.946*	3.20
Pb(22)	$Pb_{1.00}$	3.166	1.67	Sb(17)	$Sb_{0.55(4)}As_{0.45(4)}$	2.766*	2.74
M(1)	$Pb_{0.694(18)}Sb_{0.306(18)}$	3.073	2.23	As(18)	$As_{0.64(4)}Sb_{0.36(4)}$	2.527	2.57
M(2)	$Sb_{0.85(3)}Pb_{0.15(3)}$	2.992	2.39	Sb(19)	$Sb_{0.91(3)}As_{0.09(3)}$	2.585	2.52
M(3)	$Sb_{0.50}Pb_{0.50}$	3.028	2.59	As(20)	$As_{1.00}$	2.269	3.15
M(4)	$Sb_{0.898(18)}Pb_{0.102(18)}$	3.020	2.84	Sb(21a)	$Sb_{0.67}$	2.492	2.05
M(5)	$Pb_{0.589(19)}Sb_{0.411(19)}$	3.058	2.15	Sb(21b)	$Sb_{0.26}As_{0.07}$	2.459	1.03
M(6)	$Pb_{0.649(18)}Sb_{0.351(18)}$	3.032	2.31	Sb(22)	$Sb_{0.70}As_{0.30}$	2.452	3.07
M(7)	$Sb_{0.514(19)}Pb_{0.486(19)}$	2.902	2.52	Sb(23)	$Sb_{1.00}$	3.077*	2.77
M(8)	$Sb_{0.94(2)}Pb_{0.06(2)}$	3.090	2.75	Sb(24)	$Sb_{1.00}$	2.593	2.41
M(9a)	$Sb_{0.41}$	3.035	1.34	Ag(1)	$Ag_{1.00}$	2.776	1.05
M(9b)	$Pb_{0.35}Sb_{0.24}$	3.015	1.43	Ag(2)	$Ag_{1.00}$	2.792	1.04
M(10a)	$Sb_{0.47}$	3.069	1.30	Ag(3)	$Ag_{0.51(2)}Fe_{0.49(2)}$	2.700	1.68

Note: for (Sb / As)-centred sites, average distance is given by considering the three bond distances shorter than 2.75 Å. If there are less than three distances shorter than this cutoff value, the average distance is calculated on the basis of all the bond distances (indicated by *). Average distances and bond-valence sums are calculated using ECoN21 (Ilinca, 2022). The following bond parameters were used (in Å): Ag–S 2.119, As–S 2.26, Fe^{2+}–S 2.125, Pb–S 2.55, Sb–S 2.45, Tl–S 2.545. Bond parameters are from Brese and O'Keeffe (1991) for As, Pb, and Sb; from Brown and Altermatt (1985) for Ag and Tl; and from Liu and Thorp (1993) for Fe^{2+}.

bond distance. Considering also this latter bond, the average <*M*(1)–S> bond is 3.07 Å. Its site occupancy was refined to $Pb_{0.694(18)}Sb_{0.306(18)}$, with a BVS of 2.23 v.u. *M*(5) and *M*(6) sites show a monocapped trigonal prismatic coordination, with average distances of 3.06 and 3.03 Å, respectively. Site occupancies were refined to $Pb_{0.589(19)}Sb_{0.411(19)}$ and $Pb_{0.649(18)}Sb_{0.351(18)}$ for *M*(5) and *M*(6), and the BVS values are 2.15 and 2.31 v.u., respectively. Antimony-dominant positions (or with $Sb_{occ.} = Pb_{occ.}$) are *M*(2), *M*(3), *M*(4), *M*(7), and *M*(8). The *M*(2) site has three distances shorter than 3.00 Å, ranging between 2.44 and 2.95 Å, resulting in the typical trigonal pyramidal coordination of Sb^{3+} atoms. However, the average distance of these three bonds is 2.69 Å, larger than the ideal <Sb–S> distance of 2.45 Å. Additional bonds at 3.05 and 3.23 Å, with an additional long bond at 3.60 Å, complete the coordination environment. The refined site occupancy is $Sb_{0.85(2)}Pb_{0.15(2)}$, and the BVS is 2.39 v.u. The *M*(3) site has three distances between 2.71 and 2.77 Å (average 2.73 Å), with a fourth bond at 2.89 Å. There are four additional bonds between 3.03 and 3.18 Å and a longer one at 3.75 Å. The site occupancy was fixed to $Sb_{0.50}Pb_{0.50}$, and the BVS is 2.59 v.u. Probably this position is split: indeed, a trial to split it resulted in an Sb-dominant sub-site, with two short Sb–S bonds (2.44 and 2.52 Å) and two bonds around 2.80 Å, as well as a Pb-dominant sub-positions. However, since the anisotropic modelling of displacement parameters led to negatively defined values, the unsplit model is presented here. The *M*(4) site has three distances shorter than

Table 6. Bond-valence sums (in v.u.) for S sites in ginelfite.

Site	BVS	Site	BVS	Site	BVS	Site	BVS
S(1)	2.19	S(20)	1.95	S(39)	1.78	S(58)	1.58
S(2)	2.06	S(21)	1.81	S(40)	1.92	S(59)	1.98
S(3)	1.90	S(22)	2.04	S(41)	1.73	S(60)	2.04
S(4)	1.82	S(23)	1.94	S(42)	1.91	S(61)	2.07
S(5)	2.03	S(24)	2.02	S(43)	1.63	S(62)	1.53
S(6)	2.06	S(25)	2.09	S(44)	1.77	S(63)	1.82
S(7)	2.10	S(26)	2.26	S(45)	1.95	S(64)	1.82
S(8)	2.30	S(27)	1.95	S(46)	1.82	S(65)	1.96
S(9)	2.05	S(28)	1.82	S(47)	1.82	S(66)	1.83
S(10)	2.26	S(29)	1.51	S(48)	1.61	S(67)	2.32
S(11)	2.03	S(30)	1.91	S(49)	2.24	S(68)	2.04
S(12)	2.12	S(31)	1.44	S(50)	1.73	S(69)	2.05
S(13)	2.11	S(32)	2.42	S(51)	2.10	S(70)	1.69
S(14)	1.88	S(33)	1.62	S(52)	2.27	S(71)	0.60*
S(15)	2.07	S(34)	1.95	S(53)	1.78	S(72)	1.67
S(16)	1.96	S(35)	1.81	S(54)	2.38	S(73)	1.85
S(17)	2.07	S(36)	1.64	S(55)	1.71	S(74)	1.70
S(18)	2.00	S(37)	1.86	S(56)	2.13	S(75)	1.80
S(19)	2.02	S(38)	1.64	S(57)	1.75	S(76)	2.31

* Assuming half-occupancy.

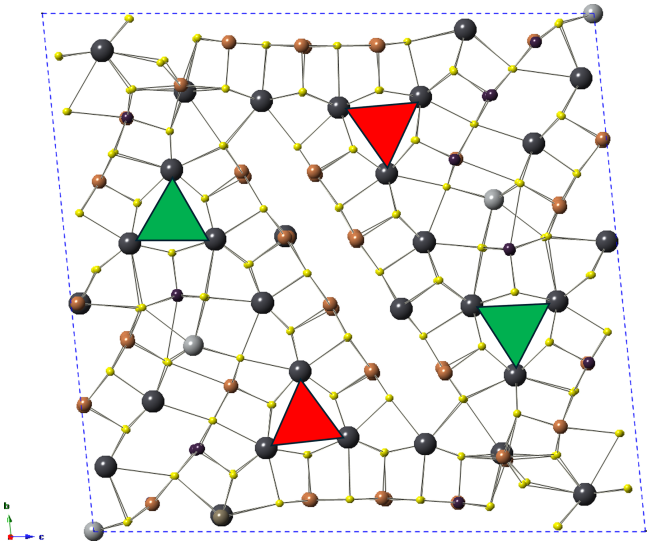

Figure 3. Unit-cell content of ginelfite. The triangular columns formed by Pb(1)–Pb(6) and Pb(7)–Pb(12) are indicated by green and red triangles, respectively.

2.8 Å (range 2.52–2.75 Å; average value 2.62 Å) and two additional ones, at 2.91 and 2.93 Å. The refined site occupancy is $Sb_{0.898(18)}Pb_{0.102(18)}$, with BVS of 2.84 v.u. The $M(7)$ site has a refined site occupancy of $Sb_{0.514(19)}Pb_{0.486(19)}$ and shows three relatively short distances (range 2.62–2.78 Å, average 2.72 Å), two additional ones around ca. 2.90 Å and a sixth (longer) bond at 3.43 Å. The BVS is 2.52 v.u. Finally, $M(8)$ is a virtually pure Sb position, with refined site occupancy $Sb_{0.94(2)}Pb_{0.06(2)}$. This site has only three distances shorter than 3.00 Å (range 2.35–2.92 Å, average 2.67 Å), but the fourth and fifth bonds are at 3.00 and 3.03 Å. Two very long distances, at ca. 3.80 Å, occur. The BVS at this site is 2.75 v.u. Among the mixed sites, four are also split, namely $M(9)$–$M(12)$. The modelling of their actual site occupancy is not straightforward. $M(9a)$ shows three short distances (range 2.42–2.71 Å, average 2.56 Å), with two additional bonds at 2.89 and 2.99 Å; its coordination is completed by three long bonds in the range 3.12–3.41 Å. This sub-position was modelled as a partially occupied Sb site. The mutually exclusive position $M(9b)$ is probably a mixed (Pb,Sb) sub-site, with a tricapped trigonal prismatic coordination, with an average bond distance of 3.02 Å. The $M(10)$ site is divided into two sub-positions, i.e. $M(10a)$ and $M(10b)$. Both sub-positions are Sb-dominant. The former has three distances in the range 2.51–2.71 Å, with two additional distances at 2.98 and 3.19 Å; a similar configuration is shown by the latter, with three distances between 2.49 and 2.80 Å, two distances at 3.02 and 3.11 Å, and a longer one at 3.53 Å. The $M(11)$ site is split into a Pb-dominant sub-site, i.e. $M(11a)$, and an Sb-dominant, i.e. $M(11b)$, sub-position. The Pb-dominant sub-site has five distances in the range 2.50–3.14 Å (three of them shorter than 2.80 Å) and two very long distances at ca. 3.90 Å. The $M(11b)$ sub-position has three short distances, ranging from 2.48 to 2.66 Å and three distances at 3.31–3.55 Å. Finally, the $M(12)$ site is Sb-dominant, with only a minor Pb content at the $M(12b)$ split position. The $M(12a)$ site shows three short distances from 2.44 to 2.58 Å, and two additional bonds at 3.23–3.24 Å, whereas the $M(12b)$ site has three bonds from 2.42 to 2.76 Å and three longer ones at 3.01, 3.25, and 3.77 Å. Details of average bond distances and BVS of these split sites are reported in Table 5.

Antimony and arsenic sites

Antimony and arsenic atoms are hosted at 24 independent positions, one of them being split. Considering bond distances shorter than 2.75 Å, the atoms hosted at these positions usually show the typical trigonal pyramidal coordination of Sb^{3+} and As^{3+} cations. However, there are some exceptions, probably due to the uncertainty in the ligand positions. Fourteen sites have $Sb_{occ.} > As_{occ.}$, whereas the remaining 10 sites have $As_{occ.} \geq Sb_{occ.}$. Sites having $Sb_{occ.} > As_{occ.}$ can be distinguished as Sb pure (eight) and mixed (Sb,As) positions (six). They usually display threefold coordination, with average $<Me–S>$ distances ranging from 2.42 Å for the mixed Sb(6) position, with an Sb / (Sb+As) atomic ratio of 0.53, to 2.59 Å for the pure Sb(24) site; BVS values range from 2.41 to 3.23 v.u. Among these sites, one, i.e. Sb(21), is split into two sub-positions. Five sites have coordination environments characterized by two distances shorter than 2.75 Å and a variable number (from one to three) of bonds between 2.75 and 3.00 Å. Further longer distances complete their coordination environments, giving BVS in the range 2.74–3.20 v.u. Among the 10 sites with $As_{occ.} \geq Sb_{occ.}$, only 1 is a pure As position, i.e. As(20), with a threefold

coordination and average distance of 2.27 Å. The other positions are mixed (As,Sb) sites, with Sb / (Sb+As) atomic ratios ranging from 0.10 to 0.50. Usually As-dominant positions have a typical threefold coordination, considering bond distances shorter than 2.75 Å, with average values between 2.27 and 2.53 Å. Bond-valence sums vary between 2.57 and 3.06 v.u. Two positions are characterized by four distances shorter than 2.75 Å, i.e. As(12) and As(15), with bond distances in the range 2.35–2.71 Å and 2.26–2.54 Å. The coordination is completed by one bond shorter than 3.30 Å. The BVS values for these two sites are 2.98 and 3.20 v.u., respectively.

Silver and mixed silver–iron sites

Silver occurs at three different positions: Ag(1), Ag(2), and Ag(3). Ag(1) and Ag(2) display a tetrahedral coordination, with four distances in the range 2.58–2.68 Å. In both cases, a fifth bond with a S atom at 3.38 and 3.44 Å for Ag(1) and Ag(2), respectively, which increases the coordination number to five, allowing the description of the coordination polyhedron as a trigonal dipyramid. Bond-valence sums at Ag(1) and Ag(2) sites are 1.05 and 1.04 v.u., in accord with the presence of Ag^{+}. The Ag(3) site is a mixed (Ag,Fe) position, with a refined site occupancy of $Ag_{0.51(2)}Fe_{0.49(2)}$. This position has four short distances, between 2.43 and 2.58 Å, and two longer ones, at ca. 3.15 Å, giving rise to a distorted octahedron. Bond-valence sum is 1.68 v.u. Below, a discussion of the possible oxidation state of Fe on the basis of structural data is given. Minor Cu detected during electron microprobe analysis was not located, but it is most likely disordered over the Ag(1) and Ag(2) positions.

Sulfur sites

Sulfur atoms occur at 76 independent positions showing variable coordination numbers (from 5 to 10, according to ECoN21; Ilinca, 2022). Bond-valence sums are usually in keeping with the occurrence of S^{2-}. Some S sites are characterized by overbonding, usually within ca. +15% of the theoretical value of 2.00 v.u., the only exception represented by S(32) that shows a deviation of +21%, having a BVS of 2.42 v.u. On the contrary, some more sites have an underbonding larger than +20%, with BVS in the range 1.44–1.58 v.u. The corresponding S atoms are bonded to mixed, and in some cases split, cation positions, and probably the underbonding is due to the average position of the ligands. An exception was the underbonding of the S(71) position, having a BVS of 1.20 v.u. This underbonding, coupled with a high U_{eq} value (0.09 $Å^2$), suggested the average position of this S site and possibly its partial occupancy. This position is bonded to some mixed and split Pb / Sb positions, namely $M(3)$ and $M(9)$. In particular, the $M(3)$ site, that was modelled as an unsplit position in the crystal structure reported in the CIF available as a Supplement, is very probably divided into two sub-positions, Sb- and Pb-dominant, respectively. The former forms an Sb–S(71) bond of 2.44(2) Å, definitely shorter than the $M(3)$–S(71) distance of 2.71(2) Å of the unsplit model. When $M(3)$ is occupied by Pb, the Pb sub-site forms a longer Pb–S(71) distance (2.85(2) Å). Moreover, the coordination environment of such a Pb atom would lead to its oversaturation; in this case, the vacancy □ at S(71) would favour a more reasonable BVS value; similarly, a shorter Sb–S distance would favour an increase in the BVS of S(71). In conclusion, the partial occupancy could be related to the substitution mechanism $2^{M(3),M(9)}Sb^{3+} + {}^{S(71)}S^{2-} = 2^{M(3),M(9)}Pb^{2+} + {}^{S(71)}\square$.

4.2.2 Oxidation state of iron

Ginelfite is characterized by the occurrence of minor Fe as a fundamental chemical constituent hosted at the Ag(3) site. A way to hypothesize the oxidation state of iron is through a comparison with other Pb sulfosalts and the use of the BVS at the Ag(3) site.

Iron is a relatively rare fundamental chemical constituent in Pb sulfosalts. The most common one is jamesonite, ideally $FePb_4Sb_6S_{14}$, where Fe occurs as Fe^{2+} in octahedral coordination, with average <Fe–S> distance in the range between 2.53 and 2.56 Å (Niizeki and Buerger, 1957; Matsushita and Ueda, 2003). Divalent iron is also reported in baiamareite, a newly described Fe^{2+} analogue of uchucchacuaite, a member of the lillianite group (Topa et al., 2023a), as well as in eclarite, where Fe occurs in tetrahedral coordination along with Cu (Topa and Makovicky, 2012), similar to what was reported for izoklakeite (actually a 4 + 2 polyhedron – Armbruster and Hummel, 1987) and pizgrischite (Meisser et al., 2007). Iron also occurs in three incommensurate minerals, i.e. cylindrite (e.g. Wang and Kuo, 1991), franckeite (e.g. Makovicky et al., 2011), and its As analogue coiraite (Paar et al., 2008). The oxidation state of Fe in franckeite was discussed by Makovicky et al. (2011), who stressed the contradictory nature of Fe, pointing out the impossibility to specify its actual oxidation state. On the contrary, Paar et al. (2008) assumed Fe^{2+} in coiraite. The only possible Pb sulfosalt with formally trivalent Fe is miharaite, where Fe occurs in tetrahedral coordination, with <Fe–S> of 2.32 Å (Petrova et al., 1988).

In ginelfite, iron occurs (along with Ag) at the mixed Ag(3) position, having a 4 + 2 octahedral coordination, with average bond distance of 2.70 Å. Refined site occupancy, $Ag_{0.51(2)}Fe_{0.49(2)}$, is in accord with electron microprobe data. Different bond-valence parameters have been given for the pairs Ag–S and Fe–S. In particular, the bond-valence parameter of the Ag–S bond was given as 2.119 Å and 2.15 Å by Brown and Altermatt (1985) and Brese and O'Keeffe (1991), respectively. The Fe–S bond-valence parameter was given as 2.16 Å by these latter authors, neglecting the oxidation state; on the contrary, Brown and Altermatt (1985) gave a bond-valence parameter of 2.143 Å for Fe^{3+}–S, whereas Liu

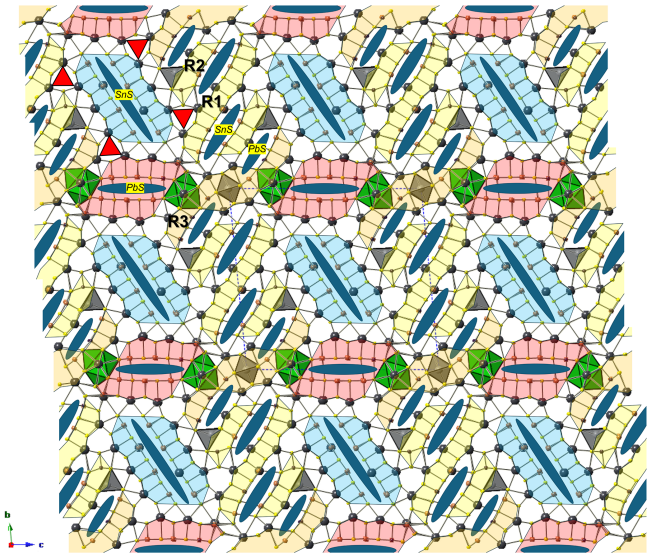

Figure 4. Organization of the crystal structure of ginelfite. Modules A, B, and C are shown in red, light blue, and yellow, respectively. Blue ellipses represent lone-electron-pair micelles. Red triangles indicate the Pb_6S_6 triangular rods. Thallium- and Ag-centred polyhedra are shown in green and grey, respectively.

and Thorp (1993) reported values of 2.125 Å and 2.134 Å for the Fe^{2+}–S and Fe^{3+}–S bonds, respectively. Finally, Brown (2020) listed the value 2.12 Å for the Fe^{2+}–S bond. The theoretical value of BVS, based on the site occupancy, should be 1.49 v.u. or 1.98 v.u. for mixed (Ag,Fe^{2+}) and (Ag,Fe^{3+}) occupancy, respectively. The BVS values calculated using different combinations of bond-valence parameters range 1.67 and 1.84 v.u., intermediate between the two possibilities. Bond-valence parameters can also be used to calculate ideal bond distances. The calculated values range 2.66–2.69 Å for mixed (Ag, Fe^{2+}) sites and between 2.59–2.61 Å for mixed (Ag,Fe^{3+}). The former distances are closer to the observed value of 2.70 Å. For this reason, the oxidation state of Fe in ginelfite can be considered +2, as with the octahedrally coordinated Fe in jamesonite.

4.2.3 Modular description of the crystal structure

The crystal structure of ginelfite is organized around two similar symmetry-independent Pb_6S_6 triangular rods (Fig. 4), typical of several zinkenite-related minerals. As with other complex zinkenite-related species, it can be described on the basis of the general approach developed by Makovicky (1993) for sulfosalts characterized by rod-based structures related to SnS and PbS archetypes. Three different modules can be distinguished, as shown in Fig. 4: two rods (A and B) and a (001) rod layer (C).

Ginelfite can be considered a new representative of the group of sulfosalts with a boxwork architecture (Makovicky and Topa, 2009). The boxwork organization can be obtained by combining three modules, i.e. walls, partitions, and fill elements, corresponding, in ginelfite, to the C, A, and B modules, respectively. The interfaces between these modules are characterized by S atoms (H-type surfaces) in front of (Pb,Tl,Sb) and S atoms (Q-type surfaces). The Pb–(Tl,Sb) atoms protrude from the Q-type surfaces and are bonded to S atoms of the H-type surfaces.

Rod A (partition) is three coordination polyhedra wide and four atomic layers thick and has the composition $Pb_4(Sb_{1.15}Pb_{0.85})_{\Sigma 2.00}(Sb_{4.83}As_{1.17})_{\Sigma 6.00}S_{15.5}\square_{0.5}$ ($=Me_{12}S_{16}$), similar to that found in other boxwork sulfosalts (e.g. scainiite – Moëlo et al., 2000 – and chovanite – Biagioni and Moëlo, 2017). Rod B (fill element) is four atomic layers thick, and its composition is $Pb_6(Sb_{3.96}Pb_{1.04})_{\Sigma 5.00}(Sb_{2.93}As_{0.07})_{\Sigma 3.00}S_{18}$ ($=Me_{14}S_{18}$). Finally, the continuous walls C can be described as formed by three different kinds of two-atomic-layer-thick ribbons, namely R1, R2, and R3. Ribbon R1 has composition $Pb_4(Sb_{1.21}Pb_{0.79})_{\Sigma 2.00}(Sb_{2.24}As_{1.76})_{\Sigma 4.00}S_{12}$ ($=Me_{10}S_{12}$). The chemical formula of ribbon R2 is $Ag_2Pb_2(Sb_{0.51}Pb_{0.49})(Sb_{2.97}As_{2.03})_{\Sigma 5.00}S_{14}$ ($=Me_{10}S_{14}$). Finally, ribbon R3 is markedly sinuous, owing to the insertion of the Ag(3)-centred octahedron. Its chemical formula can be written as $(Ag_{0.51}Fe_{0.49})(Tl_{0.65}Pb_{0.35})Pb_5(Pb_{1.24}Sb_{0.76})_{\Sigma 2.00}(As_{3.45}Sb_{2.55})_{\Sigma 6.00}S_{16}$ ($=Me_{15}S_{16}$). The continuous wall C thus has a chemical formula $(Ag_{0.51}Fe_{0.49})Ag_2(Tl_{0.65}Pb_{0.35})Pb_{11}(Pb_{2.52}Sb_{2.48})_{\Sigma 5.00}(Sb_{7.76}As_{7.24})_{\Sigma 15.00}S_{42}$.

The sum of these formulae gives $(Ag_{0.51}Fe_{0.49})Ag_2(Tl_{0.65}Pb_{0.35})Pb_{21}(Sb_{7.59}Pb_{4.41})_{\Sigma 12.00}(Sb_{15.52}As_{8.48})_{\Sigma 24.00}S_{75.5}$ ($Ev=-1.7\,\%$), which is to be compared with the ideal composition $(Ag_{2.5}Fe^{2+}_{0.5})_{\Sigma 3.00}TlPb_{24.5}(Sb_{23}As_{9.5})_{\Sigma 32.5}S_{75.5}$.

4.2.4 $(Sb,As)_mS_n$ polymerization and As versus Sb distribution

Notwithstanding the solution and refinement of the 8 Å crystal structure of ginelfite, some (Sb,As) positions are not fully resolved and, moreover, there are some mixed (and split) (Pb,Sb) positions with variable Pb / Sb atomic ratios. However, it is possible to try to select the shortest (i.e. strongest) (Sb,As)–S bonds (≤ 2.75 Å) in order to identify finite $(Sb,As)_mS_n$ groups ("polymers" – see, for instance, Moëlo et al., 2012) within the constitutive A, B, and C modules.

A module. On the left side of Fig. 5a, there is a column of mixed (Sb,Pb) positions, namely $M(3)$ and $M(9a)$–$M(9b)$, whose occupancy influences the "polymerization". If both are occupied by Sb, a possible cluster $Sb_2(As,Sb)S_6$ could occur. This polymer contains the S(71) site that, as discussed above, could be partially occupied. The $Sb_2(As,Sb)S_6$ group is followed by a probable Sb_2S_4 group. The red arrow indicates the shortest bond distance to S(38) among the longer

ones. The following polymer can be a $(Sb,As)_2S_4$ group if the bond to S(48) is selected, with a peripheral isolated SbS_3 group, or a longer $Sb(Sb,As)_2S_7$ group if the Sb(7)–S(37) bond is considered.

B module. This module is characterized by several mixed (Sb,Pb) positions, mainly concentrated in its inner portion, namely *M*(2), *M*(8), *M*(10a)–*M*(10b), and *M*(11a)–*M*(11b), whereas on the border there are the split positions *M*(12a)–*M*(12b) and Sb(21a)–Sb(21b) (Fig. 5b). *M*(12) can be considered an Sb site, with only a minor Pb content, and both sub-sites display threefold coordination, the distance between *M*(12b) and S(28) being 2.76 Å. On the contrary, Sb(23) has only two short distances, the other two with S(72) or S(70) are at 2.87 and 2.97 Å. If the relatively shorter bond is considered, a column of Sb_2S_4 composition and running along **a** can occur. It may be interrupted when *M*(12a) is occupied. The sites occurring in the inner portion of the ribbon are usually Sb-rich, with minor Pb, the only exception being represented by *M*(11a) that is Pb-dominant. *M*(8) has the site occupancy $Sb_{0.94}Pb_{0.06}$. When occupied by Sb, it probably has a threefold coordination through bonding to S(70). In this way, it could polymerize with *M*(11), when one of the sub-positions is filled by Sb. *M*(2) and *M*(10) are Sb-rich; the coordination of the former is completed through bonding with S(58), whereas the split sites *M*(10a) and *M*(10b) can be bonded to S(58) or S(31), respectively. Only a possible hypothetical polymer is shown in Fig. 5b, and it corresponds to Sb_8S_{16}. Its existence is possible only assuming the contemporaneous occupancy by Sb of the mixed and split positions.

C module. Three different ribbons have been identified in this module. On the border of ribbon R1 (Fig. 6a), the mixed Sb(11) site alternates with the mixed As(8) along **a**. The former can form a $(Sb,As)(As,Sb)SbS_7$ polymer, assuming that *M*(4) is occupied by Sb. This polymer could be bonded to the cluster $(As,Sb)SbS_4$ formed by As(8) and Sb(16), considering that the coordination of the latter could be completed through bonding with S(69) or S(43). *M*(1) is a Pb-dominant position and could interrupt the polymerization. In ribbon R2 (Fig. 6b), the polymer $As(As,Sb)SbS_7$ is followed by an Sb atom at Sb(19). The *M*(7) site is a mixed (Sb,Pb) position. When it is occupied by Pb, the Sb atoms at Sb(19) and Sb(24) remain isolated, forming two SbS_3 groups. When Sb occurs at *M*(7), some possibilities arise. Among them, the formation of an Sb_2S_4 cluster with Sb(19) or the formation, with Sb(24), of a chain of SbS_3 atoms running along **a** on the border of the ribbon, with Sb(19) remaining isolated. Finally, on the rim of ribbon R3 (Fig. 6c), isolated $(As,Sb)S_3$ groups alternate with $(As,Sb)SbS_4$ groups. In the central portion of the ribbon, a $(As,Sb)_2S_4$ polymer can be bonded to Sb(17), forming a $(As,Sb)_2(Sb,As)S_7$ cluster. Mixed *M*(5) and *M*(6) sites do not seem to be involved in polymerization with the other sites.

Comparison of Figs. 5 and 6 shows the partitioning of As among different modules. Arsenic is virtually absent in rod B, where the As / (As+Sb) atomic ratio is 0.010. It is more abundant in rod A, where the ratio is 0.164, and it is concentrated in the complex rod C, with a ratio of 0.414. Arsenic is usually concentrated in the peripheral sites, in agreement with Moëlo et al. (2012).

4.3 Crystal chemistry of ginelfite

The empirical formula of ginelfite is $Cu_{0.12}Ag_{2.51}Fe_{0.46}Tl_{0.65}Pb_{25.40}(Sb_{22.32}As_{9.54})_{\Sigma 31.86}S_{76.12}$. As discussed above, the occurrence of Cu could be related to the homovalent substitution $Cu^+ = Ag^+$, whereas Tl can be incorporated into ginelfite through the substitution $Tl^+ + (Sb,\ As)^{3+} = 2Pb^{2+}$. By subtracting Cu from the empirical formula and adding the amount of Tl necessary to completely fill one structural site, in accordance with the crystal structure study, one gets the formula $Ag_{2.63}Fe^{2+}_{0.46}Tl_{1.00}Pb_{24.70}(Sb_{22.67}As_{9.54})_{\Sigma 32.21}S_{76.12}$. This formula has an excess of $(Ag + Fe^{2+})$ of 0.09 apfu above the 3 apfu suggested by the crystal structure study (see above). This Ag excess could be hosted at some Pb positions according to the substitution $Ag^+ + Sb^{3+} = 2Pb^{2+}$. By subtracting the Ag excess, one obtains the formula $(Ag_{2.54}Fe^{2+}_{0.46})_{\Sigma 3.00}Tl_{1.00}Pb_{24.88}(Sb_{22.58}As_{9.54})_{\Sigma 32.12}S_{76.12}$. The small deficit of Fe^{2+} with respect to an ideal value of 0.5 apfu could be related to the substitution $Fe^{2+} + Pb^{2+} = Ag^+ + Sb^{3+}$. By adding the small value of 0.04 Fe apfu, the formula $(Ag_{2.50}Fe^{2+}_{0.50})_{\Sigma 3.00}Tl_{1.00}Pb_{24.92}(Sb_{22.58}As_{9.54})_{\Sigma 32.08}S_{76.12}$ is obtained.

The charge-balanced structural formula of ginelfite, assuming the full occupancy of S sites, would be $(Ag_{2.5}Fe^{2+}_{0.5})_{\Sigma 3.00}TlPb_{23.5}(Sb_{24}As_{9.5})_{\Sigma 33.5}S_{76}$ ($Z = 2$). It is worth noting that the Pb / (Sb+As) atomic ratio of this charge-balanced formula is 0.701, differing from the value obtained from the empirical formula corrected for minor substitutions, i.e. 0.777. Electron microprobe data indicate a higher Pb content than the theoretical one. Some possible crystal–chemical mechanisms favouring an increase in the Pb content could be the following ones: (i) $Sb^{3+} + \square = Pb^{2+} + Cu^+$, (ii) $Sb^{3+} + S^{2-} = Pb^{2+} + Cl^-$, or (iii) $2Sb^{3+} + \square = 3Pb^{2+}$. Substitution (i) can be discarded, as there is not enough Cu (or another monovalent cation) to justify the Pb content; similarly, no Cl was detected, and no significant amount of vacancy at cation sites is supported by the structure analysis (see above). On the contrary, a possible explanation could be related to the occurrence of anion vacancies according to the substitution $2Sb^{3+} + S^{2-} = 2Pb^{2+} + \square$. If half S vacancy occurs at S(71), as suggested by the crystal structure analysis, the ideal formula of ginelfite could be $(Ag_{2.5}Fe^{2+}_{0.5})_{\Sigma 3.00}TlPb_{24.5}(Sb_{23}As_{9.5})_{\Sigma 32.5}S_{75.5}$, with a Pb / (Sb+As) ratio of 0.754, in quite good agreement with the empirical formula.

It is interesting to compare these data with those of UM2000-44-S:AgAsPbSb (Table 2). This phase was indicated as "madocite argento-thallifère" by Moëlo

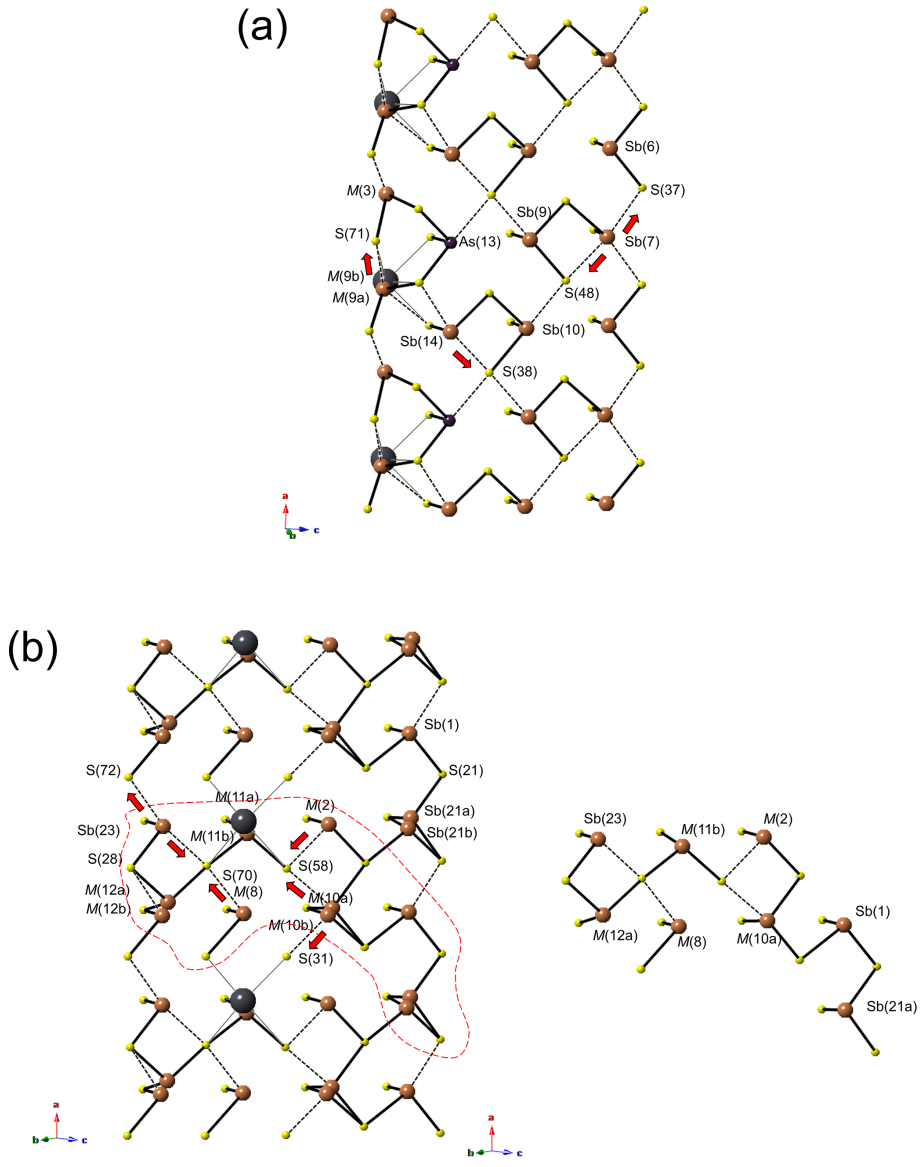

Figure 5. Polymeric organization of the (Sb,As) atoms in ginelfite in modules A **(a)** and B **(b)**. In panel **(b)**, one possible long polymer is shown (within dashed lines on left). Red arrows indicate the possible displacement of (Sb,As) atoms to achieve an ideal threefold coordination.

(1983), and in all analyses the Ag content is quite constant, ranging between ∼ 2.5 and 2.8 apfu. This author also highlighted the occurrence of low amounts of Fe (0.2 wt%). The recalculation of his chemical analyses, recalculated on the basis of $\Sigma Me = 61$ apfu, gives the formulae (i) $Ag_{2.77}Fe_{0.40}Tl_{1.48}Pb_{24.46}(Sb_{24.27}As_{7.62})_{\Sigma 31.89}S_{77.10}$, (ii) $Ag_{2.79}Fe_{0.40}Tl_{1.43}Pb_{23.69}(Sb_{24.34}As_{8.34})_{\Sigma 32.68}S_{75.47}$, and (iii) $Ag_{2.68}Fe_{0.40}Tl_{1.52}Pb_{23.95}(Sb_{24.03}As_{8.43})_{\Sigma 32.46}S_{74.59}$. By applying the substitutions $Tl^{+} + (Sb, As)^{3+} = 2Pb^{2+}$, $Ag^{+} + Sb^{3+} = 2Pb^{2+}$, and $Fe^{2+} + Pb^{2+} = Ag^{+} + Sb^{3+}$ in order to have 2.5 Ag, 0.5 Fe, and 1 Tl apfu, one obtains the Pb / (Sb+As) atomic ratios of 0.830, 0.783, and 0.795. With the exception of analysis (i), the other values are similar to those measured in ginelfite, with only a slight overestimation of Pb. It is not clear if this is due to a bias in the Pb estimation or to the occurrence of more S vacancies. On the contrary, what is clear is that Tl contents higher than those observed in ginelfite occur, possibly indicating the existence of a potential Tl-rich derivative of ginelfite.

Considering the possible substitution mechanism described above, the general formula of ginelfite could be written as $(Ag,Cu)_{2.5+x+y}Fe_{0.5-y}Tl_{1-z}Pb_{23.5-2x-y+2z+2w}(Sb,As)_{33.5+x+y-z-2w}S_{76-w}$. In the studied sample, on the basis of structural and chemical data, $x \sim 0.09$, $y \sim 0.04$, $z \sim 0.35$, and $w \sim 0.5$.

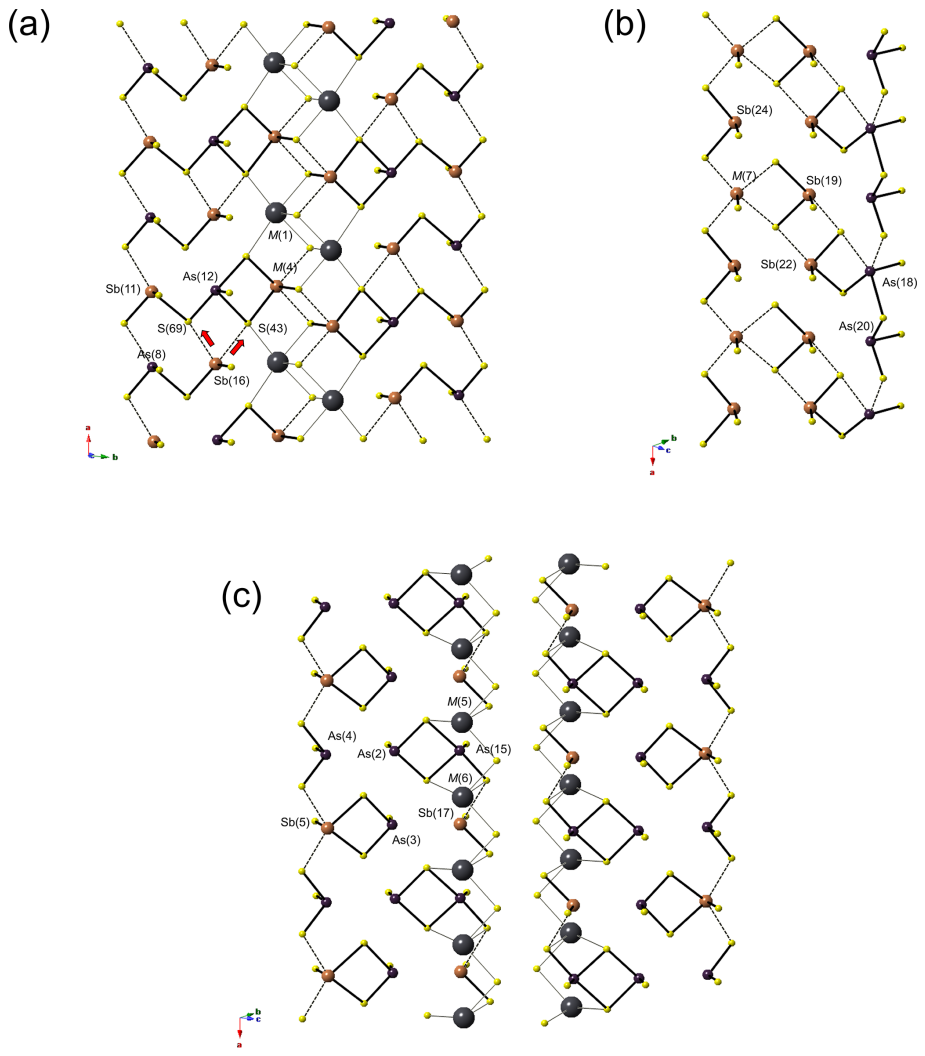

Figure 6. Polymeric organization of the (Sb,As) atoms in ginelfite in module C (ribbons R1 panel **a**, R2 panel **b**, and R3 panel **c**). Same symbols as in Fig. 5.

4.4 Relations with other species

Ginelfite belongs to the senary sulfide system Tl_2S–Ag_2S–FeS–PbS–Sb_2S_3–As_2S_3. Currently, it is the only natural member of this system. Baiamareite is the only known member of the Ag_2S–FeS–PbS–Sb_2S_3 system, and it is the Fe analogue of uchucchacuaite (Topa et al., 2023a). On the contrary, sulfosalts belonging to the system Tl_2S–Ag_2S–PbS–Sb_2S_3–As_2S_3 are relatively more common, usually belonging to the sartorite homologous series. Silver–lead sulfosalts and Tl–Pb sulfosalts are more common, but only a few of them can be classified as rod-based sulfosalts (Makovicky, 1993) such as ginelfite (Table 7). Among them, several species are related to owyheeite (Laufek et al., 2007), i.e. sardashtite and the expanded derivatives sterryite, meerschautite, parasterryite, and hayyanite (Moëlo et al., 2012; Biagioni et al., 2016; Topa et al., 2023c, d). Tubulite, with unknown crystal structure, is probably related to these species (Moëlo et al., 2013). Chukotkaite is a rod-based sulfosalt related to boulangerite (Kasatkin et al., 2020). In addition to the species listed in Table 7, there are two other species, zoubekite and rayite. The former, ideally $AgPb_4Sb_4S_{10}$, has an undetermined crystal structure and requires further studies; the latter, $(Ag,Tl)_2Pb_8Sb_8S_{21}$, originally related to the plagionite homologous series (Moëlo and Biagioni, 2020), has possibly a rod-based structure, but its crystal structure is still unknown. However, its X-ray powder diffraction pattern is different from that of ginelfite.

5 Summary and concluding remarks

During the last decade, the mineral systematics of Tl minerals (e.g. Makovicky, 2018) received great improvements, owing to the investigation of some hydrothermal ore deposits. Some of them are classic localities (e.g. Lengenbach,

Table 7. Rod-based Ag–Pb sulfosalts.

Mineral	Chemical formula	a (Å)	b (Å)	c (Å)	α (°)	β (°)	γ (°)	V (Å^3)	Ref.
Chukotkaite	$AgPb_7Sb_5S_{15}$	4.06	35.95	19.22	90	90.5	90	2804	[1]
Hayyanite	$Cu_{1.25}Ag_{2.75}Pb_{19}(Sb_{17.75}As_{4.25})_{\Sigma 22}(As_2)S_{56}$	8.19	43.05	28.63	90	90.1	90	10094	[2]
Ginelfite	$Ag_2(Ag_{0.5}Fe_{0.5})TlPb_{24.5}(Sb,As)_{32.5}S_{75.5}$	8.36	27.55	29.20	95.3	94.1	94.4	6658	[3]
Meerschautite	$Cu_{0.5}Ag_5Pb_{42}(Sb,As)_{45.5}S_{112}O^*$	8.24	43.60	28.37	90	94.1	90	10165	[4]
Owyheeite	$Ag_{1.5}Pb_{4.43}Sb_{6.07}S_{14}$	4.10	27.31	22.94	90	90.4	90	2571	[5]
Parasterryite	$Ag_4Pb_{20}(Sb,As)_{24}S_{58}$	8.40	27.95	43.88	90	90.1	90	10300	[6]
Sardashtite	$Ag_9Cu_{2.5}Pb_{41}Sb_{36.5}As_7S_{112}$	8.20	27.10	22.79	90	90.2	90	5064	[7]
Sterryite	$Cu(Ag,Cu)_3Pb_{19}(Sb,As)_{22}(As_2)S_{56}$	8.19	28.53	42.98	90	94.9	90	10005	[6]
Tubulite	$Ag_2Pb_{22}Sb_{20}S_{53}$	4.13	43.1	27.4	90	93.2	90	4872	[6]

[1] Kasatkin et al. (2020); [2] Topa et al. (2023c); [3] this study; [4] Biagioni et al. (2016); [5] Laufek et al. (2007); [6] Moëlo et al. (2012); [7] Topa et al. (2023d); [8] Moëlo et al. (2013). * Simplified to respect valence equilibrium.

Table 8. Complex Pb sulfosalts with over 100 atoms in their formula unit, and minor component (or atom pair) with atomic ratio below 1/100.

Group/Mineral	Structure type	Formula unit	No. at.	V (Å^3)	Minor component(s)	Year of definition
Boulangerite	Rod-layer					
Dadsonite		$Pb_{23}Sb_{25}S_{60}Cl$	109	2727	Cl	1979
Disulfodadsonite		$Pb_{23}Sb_{25}S_{60}$(S-S)	110	2734	S_2^*	2013
Zinkenite	Cyclic rod					
Montpelvouxite		$AgPb_{16}Sb_{27}As_{18}S_{84}$	146	3530	Ag	2022-137
Sartorite	Layer					
Interliveingite		$AgPb_{18}As_{25}S_{56}$	100	4650	Ag	2022-144
Polloneite		$AgPb_{46}Sb_{23}As_{26}S_{120}$	216	5190	Ag	2017
Dekatriasartorite		$TlPb_{58}As_{97}S_{204}$	360	8477	Tl	2017
Hendekasartorite		$Tl_2Pb_{48}As_{82}S_{172}$	304	7076	Tl	2017
Chabournéite	Layer					
Vallouiseite		$Ag_3Tl_{21.5}PbSb_{63}As_{41.5}S_{170}$	300	7331	Ag, Pb	2023-051
Sterryite	Chessboard					
Sterryite		$Cu(Ag,Cu)_3Pb_{19}(Sb,As)_{22}$(As-As)$S_{56}$	103	10005	Cu, As_2^*	2011
Meerschautite		$Ag_5Cu_{0.5}Pb_{42}(Sb,As)_{45.5}S_{112}O$	206	10165	O (Cu?)	2016
Hayyanite		$Cu_{1.25}Ag_{2.75}Pb_{19}(Sb_{17.75}As_{4.25})_{\Sigma 22}$(As-As)$S_{56}$	103	10094	Cu, As_2^*	2023
	Boxwork					
Pellouxite		$(Cu,Ag)_2Pb_{21}Sb_{23}S_{55}ClO$	103	5065	Cl, O	2004
Rouxelite		$Cu_2HgPb_{22}Sb_{28}S_{64}(O,S)_2$	119	5887	Hg, O	2005
Ginelfite		$Ag_2(Ag_{0.5}Fe_{0.5})TlPb_{24.5}(Sb,As)_{32.5}S_{76}$	137	6658	Fe, Tl	2022-110

Note: No. at. is the number of atoms. * $(As_2)^{4+}$ and $(S_2)^{2-}$ groups are considered single units. The question mark represents uncertainty.

Jas Roux), whereas others have been discovered only in the last 15 years (e.g. Monte Arsiccio, Vorontsovskoe).

This study illustrated the ability of thallium to be hosted in several different structural arrangements, among which the most complex among sulfosalts, i.e., the boxwork structures (Makovicky and Topa, 2009). Biagioni et al. (2014, 2018b) and Biagioni and Moëlo (2017) discussed the occurrence of Tl in rouxelite and chovanite from the Monte Arsiccio mine. The Tl-bearing variety of chovanite, with ideal formula $TlPb_{26}(Sb,As)_{31}S_{72}O$, has Tl disordered over two Pb-dominant positions, thus precluding its proposal as a distinct mineral species (Biagioni et al., 2018b). On the contrary, no structural data are currently available for Tl-bearing rouxelite, that has up to 0.83 Tl apfu (Biagioni et al., 2014) and could be a possible candidate for being a new Tl sulfosalt. Ginelfite, with Tl fully ordered at one site and with a new structure type, is the first example of a Tl species with a boxwork structure. Moreover, the high As content may indicate that this element is necessary for the stability of ginelfite and thus, as remarked above, it would be the so far only known natural example of a compound belonging to the senary system Tl_2S–Ag_2S–FeS–PbS–Sb_2S_3–As_2S_3.

Its identification further highlights the importance of the study of the mineral assemblages of hydrothermal systems,

where subtle physicochemical changes can favour the crystallization of totally unexpected new structure types (e.g. Moëlo et al., 2012), whose complexity can be revealed by the new generation of single-crystal X-ray diffractometers.

Table 8 lists the 14 Pb sulfosalts of this type with over 100 atoms in their formula unit, where at least one minor component (*Mc*) has an atomic ratio below 1/100. All species except dadsonite have been discovered recently (since 2011). Such improbable compounds of the sulfide class point to fundamental questions that are difficult to solve today:

- *Stability.* How does such a minor component permit an energy benefit over a composition without *Mc*?
- *Crystal genesis.* What is the building process starting from dispersed ions in the hydrothermal solution up to the first unit-cell group (initiation) and then the 3D growth of the structure (germination)?

Modular analysis, as presented here and in previous studies of such complex structures, constitutes a useful approach for these two challenges.

Data availability. Crystallographic data for ginelfite are available in the Supplement.

Supplement. The supplement related to this article is available online at https://doi.org/10.5194/ejm-37-319-2025-supplement.

Author contributions. CB, GF, VB, and J-CB: conception of the project; JS and JU: electron probe microanalysis and optical measurements; CB and SM: single-crystal X-ray measurements, data interpretation; CB and YM: data interpretation and writing of the paper with inputs from other authors.

Competing interests. At least one of the (co-)authors is a member of the editorial board of *European Journal of Mineralogy*.

Disclaimer. Publisher's note: Copernicus Publications remains neutral with regard to jurisdictional claims made in the text, published maps, institutional affiliations, or any other geographical representation in this paper. While Copernicus Publications makes every effort to include appropriate place names, the final responsibility lies with the authors.

Special issue statement. This article is part of the special issue "Celebrating the outstanding contribution of Paola Bonazzi to mineralogy". It is not associated with a conference.

Acknowledgements. This paper is dedicated to the loving memory of Paola Bonazzi (1960–2024). We appreciate the many constructive comments of Dan Topa and an anonymous reviewer, as well as the suggestions of the associate editor Luca Bindi and the chief editor Elisabetta Rampone, who helped us to improve this paper. The Centro per l'Integrazione della Strumentazione Scientifica dell'Università di Pisa (C.I.S.U.P.) is thanked for access to the single-crystal X-ray diffraction laboratory.

Financial support. This research was supported by the Ministry of Culture of the Czech Republic (long-term project DKRVO 2024-2028/1.II.b; National Museum, 00023272) for Jiří Sejkora and Jana Ulmanová.

Review statement. This paper was edited by Luca Bindi and reviewed by Dan Topa and one anonymous referee.

References

Armbruster, T. and Hummel, W.: (Sb,Bi,Pb) ordering in sulfosalts: Crystal-structure refinement of a Bi-rich izoklakeite, Am. Mineral., 72, 821–831, 1987.

Biagioni, C. and Moëlo, Y.: Lead-antimony sulfosalts from Tuscany (Italy). XIX. Crystal chemistry of chovanite from two new occurrences in the Apuan Alps and its 8 Å crystal structure, Mineral. Mag., 81, 811–831, 2017.

Biagioni, C., Moëlo, Y., and Orlandi, P.: Lead-antimony sulfosalts from Tuscany (Italy). XV. (Tl-Ag)-bearing rouxelite from Monte Arsiccio mine: occurrence and crystal chemistry, Mineral. Mag., 78, 651–661, 2014.

Biagioni, C., Moëlo, Y., Orlandi, P., and Stanley, C.J.: Lead-antimony sulfosalts from Tuscany (Italy). XVII. Meerschautite, $(Ag,Cu)_{5.5}Pb_{42.4}(Sb,As)_{45.1}S_{112}O_{0.8}$, a new expanded derivative of owyheeite from the Pollone mine, Valdicastello Carducci: occurrence and crystal structure, Mineral. Mag., 80, 675–690, 2016.

Biagioni, C., Bindi, L., and Moëlo, Y.: Another step toward the solution of the real structure of zinkenite, Z. Kristallogr., 233, 269–277, 2018a.

Biagioni, C., Moëlo, Y., Perchiazzi, N., Demitri, N., and Lepore, G. O.: Lead-antimony sulfosalts from Tuscany (Italy). XXIV. Crystal structure of thallium-bearing chovanite, $TlPb_{26}(Sb,As)_{31}S_{72}O$, from the Monte Arsiccio mine, Apuan Alps, Minerals, 8, 535, https://doi.org/10.3390/min8110535, 2018b.

Biagioni, C., D'Orazio, M., Fulignati, P., George, L.L., Mauro, D., and Zaccarini, F.: Sulfide melts in ore deposits from low-grade metamorphic settings: Insights from fluid and Tl-rich sulfosalt microinclusions from the Monte Arsiccio mine (Apuan Alps, Tuscany, Italy), Ore Geol. Rev., 123, 103589, https://doi.org/10.1016/j.oregeorev.2020.103589, 2020.

Bindi, L., Biagioni, C., Förster, H. J., and Adelmann, H. G.: Markwelchite, $TlPbSbS_3$, a new Tl-Pb sulfosalt from the hydrothermal deposit of Jas Roux, Hautes-Alpes, France, Mineral. Mag., 88, 503–509, https://doi.org/10.1180/mgm.2024.43, 2024.

Boev, B., Bermanec, V., Serafimovski, T., Lepitkova, S., Mikulčić, S., Šoufek, M., Jovanovski, G., Stafilov, T., and Najdoski, M.:

Allchar mineral assemblage, Geol. Macedonica, 15-16, 1–16, 2001–2002.

Bolte, M.: *TWINLAW* and *HKLF*5: two programs for the handling of non-merohedral twins, J. Appl. Crystallogr., 37, 162–165, 2004.

Bourgoin, V., Favreau, G., and Boulliard, J. C.: Jas Roux (Hautes-Alpes): un gisement exceptionnel à minéraux de thallium, Le Cahier des Micromonteurs, 113, 1–92, 2011.

Brese, N. E. and O'Keeffe, M.: Bond-valence parameters for solids, Acta Crystallogr., B47, 192–197, 1991.

Brown, I. D.: Accumulated table of bond valence parameters, https://www.iucr.org/resources/data/datasets/bond-valence-parameters (last access: August 2024), 2020.

Brown, I. D. and Altermatt, D.: Bond-valence parameters obtained from a systematic analysis of the Inorganic Crystal Structure Database, Acta Crystallogr., B41, 244–247, 1985.

Guillemin, C., Johan, Z., Laforêt, C., and Picot, P.: La pierrotite $Tl_2(Sb,As)_{10}S_{17}$ une nouvelle espèce minérale, Bull. Soc. Fr. Minéral. Cristallogr., 93, 66–71, 1970.

Hawthorne, F. C., Ungaretti, L., and Oberti, R.: Site populations in minerals: terminology and presentation of results of crystal-structure refinement, Can. Mineral., 33, 907–911, 1995.

Ilinca, G.: Charge distribution and bond valence sum analysis of sulfosalts – The ECoN21 computer program, Minerals, 12, 924, https://doi.org/10.3390/min12080924, 2022.

Johan, Z. and Mantienne, J.: Thallium-rich mineralization at Jas Roux, Hautes-Alpes, France: a complex epithermal, sediment-hosted, ore-forming system, J. Czech Geol. Soc., 45, 63–77, 2000.

Johan, Z., Mantienne, J., and Picot, P.: La routhierite, $TlHgAsS_3$, et la laffittite, $AgHgAsS_3$, deux nouvelles espèces minérales, Bull. Soc. Fr. Minéral. Cristallogr., 97, 48–53, 1974.

Johan, Z., Mantienne, J., and Picot, P.: La chabournéite, un nouveau mineral thallifère, Bull. Minéral., 104, 10–15, 1981.

Liu, W. and Thorp, H. H.: Bond valence sum analysis of metal-ligand bond lengths in metalloenzymes and model complexes. 2. Refined distances and other enzymes, Inorg. Chem., 32, 4102–4105, 1993.

Kasatkin, A. V., Makovicky, E., Plášil, J., Škoda, R., Agakhanov, A. A., Chaikovskiy, I. I., Vlasov, E. A., and Pekov, I.V.: Chukotkaite, $AgPb_7Sb_5S_{15}$, a new sulfosalt mineral from Eastern Chukotka, Russia, Can. Mineral., 58, 587–596, 2020.

Kraus, W. and Nolze, G.: POWDER CELL – a program for the representation and manipulation of crystal structures and calculation of the resulting X-ray powder patterns, J. Appl. Crystallogr., 29, 301–303, 1996.

Laufek, F., Pažout, R., and Makovicky, E.: Crystal structure of owyheeite, $Ag_{1.5}Pb_{4.43}Sb_{6.07}S_{14}$: refinement from powder synchrotron X-ray diffraction, Eur. J. Mineral., 19, 557–566, 2007.

Makovicky, E: Rod-based sulphosalt structures derived from the SnS and PbS archetype, Eur. J. Mineral., 5, 545–591, 1993.

Makovicky, E.: Modular crystal chemistry of thallium sulfosalts, Minerals, 8, 478, https://doi.org/10.3390/min8110478, 2018.

Makovicky, E. and Topa, D.: The crystal structure of sulfosalts with boxwork architecture and their new representative, $Pb_{15-2}xSb_{14+2}xS_{36}O_x$, Can. Mineral., 47, 3–24, 2009.

Makovicky, E., Petříček, V., Dušek, M., and Topa, D.: The crystal structure of franckeite, $Pb_{21.7}Sn_{9.3}Fe_{4.0}Sb_{8.1}S_{56.9}$, Am. Mineral., 96, 1686–1702, 2011.

Mantienne, J.: La minéralisation thallifère de Jas-Roux (Hautes-Alpes), Thèse Doct. Université de Paris, 153 p., 1974.

Matsushita, Y. and Ueda, Y.: Structure and physical properties of 1D magnetic chalcogenide, jamesonite ($FePb_4Sb_6S_{14}$), Inorg. Chem., 42, 7830–7838, 2003.

Meisser, N., Schenk, K., Berlepsch, P., Brugger, J., Bonin, M., Criddle, A.J., Thélin, P., and Bussy, F.: Pizgrischite, $(Cu,Fe)Cu_{14}PbBi_{17}S_{35}$, a new sulfosalt from the Swiss Alps: description, crystal structure and occurrence, Can. Mineral., 45, 1229–1245, 2007.

Moëlo, Y.: Contribution à l'étude des conditions naturelles de formation des sulfures complexes d'antimoine et plomb (sulfosels de Pb / Sb). Signification métallogénique, Série Documents du BRGM, 55, 624 pp., 1983.

Moëlo, Y. and Biagioni, C.: Contribution to the crystal chemistry of lead-antimony sulfosalts: systematic Pb-versus-Sb crossed substitution in the plagionite homologous series, $Pb_{2N-1}(Pb_{1-x}Sb_x)(Sb_{1-x}Pb_x)_2Sb_6S_{13+2N}$, Eur. J. Mineral., 32, 623–635, 2020.

Moëlo, Y., Meerschaut, A., and Makovicky, E.: Refinement of the crystal structure of nuffieldite, $Pb_2Cu_{1.4}(Pb_{0.4}Bi_{0.4}Sb_{0.2})Bi_2S_7$: structural relationships and genesis of complex lead sulfosalt structures, Can. Mineral., 35, 1497–1508, 1997.

Moëlo, Y., Meerschaut, A., Orlandi, P., and Palvadeau, P.: Lead-antimony sulfosalts from Tuscany (Italy): II – Crystal structure of scainiite, $Pb_{14}Sb_{30}S_{54}O_5$, an expanded derivative of $Ba_{12}Bi_{24}S_{48}$ hexagonal sub-type (zinkenite group), Eur. J. Mineral., 12, 835–846, 2000.

Moëlo, Y., Guillot-Deudon, C., Evain, M., Orlandi, P., and Biagioni, C.: Comparative modular analysis of two complex sulfosalt structures: sterryite, $Cu(Ag,Cu)_3Pb_{19}(Sb,As)_{22}(As–As)S_{56}$, and parasterryite, $Ag_4Pb_{20}(Sb,As)_{24}S_{58}$, Acta Crystallogr., B68, 480–492, 2012.

Moëlo, Y., Pecorini, R., Ciriotti, M.E., Meisser, N., Caldes, M.T., Orlandi, P., Petit, P.-E., Martini, B., and Salvetti, A.: Tubulite, $\sim Ag_2Pb_{22}Sb_{20}S_{53}$, a new Pb–Ag–Sb sulfosalt from Le Rivet quarry, Peyrebrune ore field (Tarn, France) and Biò, Borgofranco mines, Borgofranco d'Ivrea (Piedmont, Italy), Eur. J. Mineral., 25, 1017–1030, 2013.

Niizeki, N. and Buerger, M. J.: The crystal structure of jamesonite, $FePb_4Sb_6S_{14}$, Z. Kristallogr., 109, 161–183, 1957.

Paar, W. H., Moëlo, Y., Mozgova, N. N., Organova, N. I., Stanley, C. J., Roberts, A. C., Culetto, F. J., Effenberger, H. S., Topa, D., Putz, H., Sureda, R. J., and de Brodtkorb, M. K.: Coiraite, $(Pn,Sn^{2+})_{12.5}As_3Fe^{2+}Sn_5^{4+}S_{28}$: a franckeite-type new mineral species from Jujuy Province, NW Argentina, Mineral. Mag., 72, 1083–1101, 2008.

Petrova, I. V., Pobedimskaya, E. A., and Bryzgalov, I. A.: Crystal structure of miharaite $Cu_4FePbBiS_6$, Dokl. Akad. Nauk SSSR, 299, 123–127, 1988 (in Russian).

Pouchou, J. L. and Pichoir, F.: "PAP" ($\varphi\rho$Z) procedure for improved quantitative microanalysis, Pp. 104–106 in: Microbeam Analysis, edited by: Armstrong, J. T., San Francisco Press, San Francisco, 1985.

Raber, T. and Roth, P.: The Lengenbach quarry in Switzerland: classic locality for rare thallium sulfosalts, Minerals, 8, 409, https://doi.org/10.3390/min8090409, 2018.

Sheldrick, G. M.: SHELXT – Integrated space-group and crystal-structure determination, Acta Crystallogr., A71, 3–8, 2015a.

Sheldrick, G. M.: Crystal structure refinement with SHELXL, Acta Crystallogr., C71, 3–8, 2015b.

Smith, D. G. W. and Nickel, E. H.: A system for codification for unnamed minerals: report of the Subcommittee for Unnamed Minerals of the IMA Commission on New Minerals, Nomenclature and Classification, Can. Mineral., 45, 983–1055, 2007.

Topa, D. and Makovicky, E.: Eclarite: new data and interpretations, Can. Mineral., 50, 371–386, 2012.

Topa, D., Makovicky, E., Favreau, G., Bourgoin, V., Boulliard, J. C., Zagler, C., and Putz, H.: Jasrouxite, a new Pb-Ag-As-Sb member of the lillianite homologous series from Jas Roux, Hautes-Alpes, France, Eur. J. Mineral., 25, 1031–1038, 2013a.

Topa, D., Makovicky, E., Putz, H., and Zagler, G.: Lopatkaite, IMA 2012-083. CNMNC Newsletter 15, Mineral. Mag., 77, 1–12, 2013b.

Topa, D., Kolitsch, U., Makovicky, E., and Stanley, C.: Écrinsite, $AgTl_3Pb_4As_{11}Sb_9S_{36}$, a new thallium-rich homeotype of baumhauerite from the Jas Roux sulphosalt deposit, Parc national des Écrins, Hautes-Alpes, France, Eur. J. Mineral., 29, 689–700, 2017.

Topa, D., Kolitsch, U., Stoeger, B., Keutsch, F., and Stanley, C.: Dewitite, IMA 2019-098. CNMNC Newsletter 63, Eur. J. Mineral., 33, 639–646, 2020.

Topa, D., Sicher, P., Keutsch, F., Kolitsch, U., and Stanley, C.: Baiamareite, IMA 2023-044, CNMNC Newsletter 75, Eur. J. Mineral., 35, 891–895, 2023a.

Topa, D., Stoeger, B., Kolitsch, U., Keutsch, F., Stanley, C., and Raber, T.: Vallouiseite, IMA 2023-051. CNMNC Newsletter 75, Eur. J. Mineral., 35, 891–895, 2023b.

Topa, D., Stoeger, B., Kolitsch, U., Keutsch, F., and Stanley, C.: Hayyanite, IMA 2023-048. CNMNC Newsletter 75, Eur. J. Mineral., 35, 891–895, 2023c.

Topa, D., Stoeger, B., Kolitsch, U., Keutsch, F., and Stanley, C.: Sardashtite, IMA 2022-140. CNMNC Newsletter 72, Eur. J. Mineral., 35, 285–293, 2023d.

Topa, D., Stoeger, B., Kolitsch, U., and Stanley, C.J.: Montpelvouxite, IMA 2022-137, CNMNC Newsletter 72, Eur. J. Mineral., 35, 285–293, 2023e.

Wang, S. and Kuo, K. H.: Crystal lattices and crystal chemistry of cylindrite and franckeite, Acta Crystallogr., A47, 381–392, 1991.

Warr, L. N.: IMA-CNMNC approved mineral symbols, Mineral. Mag., 85, 291–320, 2021.

Wilson, A. J. C. (editor): International Tables for Crystallography Volume C: Mathematical, Physical and Chemical Tables, Kluwer Academic Publishers, Dordrecht, The Netherlands, 1992.